Ionospheric Tomography Using GPS Measurements

Zhizhao Liu and Yang Gao

Department of Geomatics Engineering
The University of Calgary
Calgary, Alberta Canada T2N 1N4
Tel: 403-220-6174 Fax: 403-284-1980
Email: zzliu@ucalgary.ca

BIOGRAPHY

Mr. Zhizhao Liu is a Ph.D student at the Department of Geomatics Engineering, The University of Calgary. His current research interests include atmosphere modeling using GPS data and precise GPS geodetic positioning.

Dr. Yang Gao is an Assistant Professor at the Department of Geomatics Engineering, The University of Calgary. His research focuses on satellite navigation and wireless mobile information management systems.

ABSTRACT

Single layer ionosphere model, essentially 2-dimensional model, has been widely used for ionosphere modeling and estimation using GPS measurements from a network of multiple reference stations. Using such a model, the electrons in the ionosphere are assumed to concentrate on a thin ionosphere shell located at an altitude of about 350 km above the earth. The shortcoming of this type of model is that it can't retrieve information of the ionospheric vertical profile. Therefore the obtainable accuracy of ionospheric correction in GPS positioning using 2D model is restricted by its inherent characteristics. To further improve the accuracy of the ionosphere estimates and to monitor the ionospheric spatio-temporal variations, the single layer model should be expanded to multi-layer models. This paper will discuss the development of a three-dimensional (3D) ionosphere model using tomography methodology so that ionospheric electron densities can be estimated at layers of different altitudes. Ionospheric tomography can be modeled horizontally by a series of harmonics functions and vertically by empirical orthogonal functions (EOFs) using the total electron content (TEC) computed from GPS observations. The number of ionosphere layers depends on the resolution requirement and the density of the GPS ionosphere measurements. Numerical results will be presented using GPS data from an operational GPS reference network. The total electron contents derived from the tomography model will be compared with the TEC measurements directly derived from the dual frequency GPS data to assess the performance of the ionospheric tomography model. Our research results have shown that the new model can recover about 90 percent of the total electron content. The ionosphere electron densities at different altitudes are computed based on the coefficients from the tomography model, which indicates the strength of 3D modeling over the 2D modeling.

1 INTRODUCTION

Ionospheric delay, as a pronounced error in GPS positioning and navigation especially in the high geomagnetic activity period, has long been extensively studied, for example, Brunner and Gu [1991], King et al. [1985], Klobuchar [1986], etc. The ionosphere delay should be corrected in order to get a precise positioning and navigation results using GPS. For the ionospheric correction, typically two methods exist in GPS applications. One is the use of dual-frequency GPS data to eliminate the ionospheric effects taking advantage of the ionospheric dispersive feature. The other way is to employ a regional or global network of GPS reference receivers to model the ionosphere and then GPS users use the model to correct the ionospheric delay. The advantage of the latter method is obvious because it can provide ionospheric correction service to numerous GPS users within the coverage area in a cost-effective mode. The network ionospheric correction is particularly useful for single frequency GPS receiver because it can't use dual-frequency data to correct ionospheric delay and the Klobuchar model correction using broadcast ionosphere parameters can

only correct about 50% error. It is apparently seen a number of regional GPS reference networks are increasingly emerging in many nations in the world, e.g. SWEPOS of Sweden, CACS of Canada, and WAAS of USA. The emergence of those regional GPS networks gives a solid basis for ionospheric modeling.

Various two dimensional (2D) ionospheric modeling techniques have been investigated. Ionospheric grid algorithm was developed by MITRE and the Air Force Phillips Laboratory (AFPL) [El-Arini et al., 1993, 1994a]. Grid algorithm was compared with other non-grid models, including least squares fit, spherical harmonic model, spherical cap harmonic model, and adjusted spherical harmonic model by [El-Arini, et al., 1994b]. Comparison results from El-Arini et al.[1994b] indicated the model prediction accuracy degraded with the decrement of elevation angles and the slant range prediction error at elevation angle of 15 degree was at 2 meter level. A common feature in these models is that a single thin ionosphere shell at a given altitude, say 350km, above the Earth is assumed. This assumption has two aspects of drawbacks. One is that this assumption is not strictly true to the physical fact. Ionosphere covers the region between approximately 50 and 1500km above the Earth's surface. The second drawback is that not taking the variability of the single shell height into account would introduce an error of several TECU [Komjathy, 1997].

This paper aims to establish a three dimensional (3D) ionospheric model using tomographic technique with the global positioning system (GPS) measurements. Ionospheric tomography includes two basic steps. One is the calculation of total electron content (TEC). The other is called model inversion in which a set of model coefficients is derived.

Three-dimensional (3D) ionospheric model has an apparent strength over 2D model. 3D model describes the ionosphere in the full dimensions of the space, unlike the 2D one which simply presumes the ionosphere concentrating in a single thin shell and obviously biases from the physical fact. Therefore the 3D model doesn't have the drawbacks coherent with 2D models. Another merit of using 3D model is the feasibility of monitoring and predicting the 3D spatial ionospheric variation with time.

Because the three-dimensional ionospheric model describes the characteristics of the entire ionosphere, rather than only a single shell, it is expected 3D model has an enhancement in terms of ionosphere model's recovery capability compared with 2D models. The results of this study show that the 3D model can averagely recover 90% ionospheric delays at various elevations, even using only GPS pseudorange measurements as model inputs.

In the section 2, the 3D ionospheric modeling and tomographic technique are described in detail. The methodology of 3D modeling is given. In section 3, an experiment made with the data from the Southern California Integrated GPS Network (SCIGN). GPS data from 11 reference stations of SCIGN network is processed and a 3D ionospheric model is established. The model is examined by comparing the model predicted TEC values with those derived from GPS data. The ionosphere electron density distributions for various layers at different altitudes are computed based on the constructed tomography model. Some conclusions are drawn at the end of this paper.

2 3D IONOSPHERIC MODEL

Three-dimensional (3D) ionospheric model has a strength superior to the two dimensional (2D) ones because it characterizes not only the ionospheric horizontal profile but also the vertical one while 2D models only provide horizontal profile at a fixed altitude above the Earth. Generally two methods exist to expand the 2D model to the 3D one.

One method is to use tomography technique to construct the ionospheric spatial structure. The other method takes advantage of voxel (pixel) technique to divide the ionosphere into many small voxels. On the average, voxel method is more conceptually straightforward but more complex in terms of programming implementation and computation. The ionospheric tomography is much easier in terms of programming computation and more efficient in ionospheric recovering. Usually the voxel technique needs less GPS measurements to model than the tomography technique required. Therefore the former method usually method has higher time resolution than the latter one.

Tomography is a two-step process. First, integral measurements are made of the medium of interest, ideally along many paths at many different viewing angles. Second, these integral measurements are inverted to obtain an estimate of the field [Howe et al., 1998]. A tomographic system has two strengths relative to conventional in situ point measurements. First, as instruments are added, the amount of data goes up roughly quadratically; under ideal circumstances, the amount of data grows as the product of the number of sources and the number of receivers. The second strength lies in the integral,

path-averaging nature of the basic measurement. [Howe, 1997].

The 3D ionospheric model utilizing the tomography technique is constructed horizontally by harmonics function and vertically by the empirical orthogonal functions (EOFs). The function is mainly built by the first several orders of harmonics. The high-order harmonics improve the sharpness of the fronts. EOFs are derived from an existing data set (observation data or model data) of the medium of our interest. The advantages of employing EOFs are [Secan and Tascione, 1984]:

1) Although any orthogonal function set may be used to fit a data set, the EOFs of the data set provide the least RMS error for a given number of terms in the expansion; and
2) In practice, the first few EOFs of the data set typically describe most of the variance of the data set [Lorentz, 1956; Kutzbach, 1967].

Austen et al. [1986] first applied the tomography technique to the ionospheric imaging. Later on extensive studies were done on this ionospheric tomography, see Austen et al. [1988], Raymund et al. [1990, 1994, 1995], Fremouw et al. [1992], Andreeva et al. [1992], Kersley et al. [1993] Hansen et al. [1997], Howe et al. [1998]. However most investigators, for instance Austen et al. [1988], Raymund et al. [1994], Kersley et al. [1993], and Andreeva et al. [1992], used the total electron content (TEC) measurements collected by a chain of meridionally aligned stations all simultaneously observing a rapidly orbiting radio beacon. The drawback associated with this configuration is that the geometry distribution of TEC observations is rather weak in the solution. In Howe [1997] and Howe et al. [1998], only simulated GPS data instead of using real GPS data.

The methodology of ionospheric tomography is developed in the following section and it is implemented using a group of real-world GPS data to construct a 3D dimensional ionospheric model. The experiment result validates the feasibility of the ionospheric tomography method.

3 METHODOLOGY

The procedure of ionospheric tomography consists of two parts, namely model measurement TEC derivation and model parameter inversion. The model measurements are derived from processing GPS data. Then the measurements are used as input to tomographic mode to solve the model parameters.

3.1 TEC ESTIMATION

Ionospheric models usually have the total electron content (TEC) data as input observations, which in most cases are calculated from a GPS reference network. The ionosphere is a dispersive medium and the electromagnetic wave propagating through it suffers a phase delay whose size depends on the frequency of the wave. The index of ionosphere is given by Appleton-Hartree equation [Hargreaves, 1992]. For L-band GPS signals, the following expression is a good approximation for index of ionosphere. [Parkinson and Spilker, 1996].

$$n(r, f, t) = 1 - \frac{e^2 N_e(r)}{4p e_0 m f} + O(1/f^3) \quad (1)$$

where e is the charge of on an electron; $N_e(r)$ is the local electron density; e_0 is the permittivity in free space; m is the mass of an electron and f is the frequency of the electromagnetic wave. The fact that the value of index of ionosphere differs from 1 results in the deviation of GPS signal velocity in the space from ideal light velocity c_0 . The difference in velocity multiplied by signal propagation time can be converted into a range error which can be formulated by:

$$\Delta R = \pm 40.3 \frac{TEC}{f^2} \quad (2)$$

For carrier phase measurement the minus sign is used while for pseudorange measurement the positive correction is applied.

Using Eq. (2) and the pseudorange measurements from two different frequencies, TEC can be readily solved by:

$$\text{TEC} = \frac{f_1^2 f_2^2 (R_1 - R_2)}{40.3(f_2^2 - f_1^2)} \quad (3)$$

where R_i and f_i $(i = 1,2)$ are the pseudorange and the corresponding frequency, respectively.

However in Eq. (3), the receiver/satellite biases implicitly existing in pseudorange measurements are not taken into account. The GPS instrumental biases affect the line-of-sight ionospheric delay measurements derived from differencing dual-frequency pseudorange data [Gao et al., 1994]. This is because the L_1 and L_2 phase paths between the antenna and the correlation loops in both the receiver and the GPS satellite transmitter are different. The differences corrupt the ionospheric measurements by introducing the interfrequency biases from both receiver and satellite. If the two biases are not removed, GPS data generate only relative rather than

absolute TEC values. Gao et al. [1994] showed that the receiver bias can be as large as 10 nanoseconds and satellite bias can be as large as a few nanoseconds. To account for the effects of instrumental biases, Eq. (3) is modified to:

$$\begin{aligned} \text{TEC} &= \frac{f_1^2 f_2^2 (R_1 - R_2 - b_{rx} - b_{sv})}{40.3(f_2^2 - f_1^2)} \\ &= -9.52 \times 10^{16} (R_1 - R_2 - b_{rx} - b_{sv}) \end{aligned} \quad (4)$$

where b_{rx} and b_{sv} are the receiver interfrequency bias and satellite interfrequency bias, respectively.

To reduce the magnitude of noise level in TEC measurements, GPS pseudorange data can be smoothed with the assimilation of carrier phase data. A first investigation on the carrier phase and code pseudorange measurement combination was provided by Hatch [1982]. Lachapelle et al. [1986] gave a varied weighted algorithm of smoothing code pseudorange with carrier phase measurements.

$$R(t_i)_{sm} = wR(t_i) + (1-w)[R(t_{i-1})_{sm} + j(t_i) - j(t_{i-1})] \quad (5)$$

where $R(t_i)_{sm}$ is the smoothed code pseudorange at time t_i, unit in cycle; $R(t_i)$ is the measured code pseudorange observation at time t_i, unit in cycle; $j(t_i)$ is the measured carrier phase observation at time t_i, unit in cycle; w is the time dependent weight factor with an initial value of 1.

Lachapelle et al. [1986] proposed a reduction of the weight by 0.01 from epoch to epoch for a kinematic experiment with a data sampling rate of 1Hz. This algorithm fails when cycle slips occur. After the occurrence of a cycle slip, the weight is reset to w = 1 which fully eliminates the influence of the erroneous carrier phase data. The key of this approach is that cycle slips must be detected but do not have to be corrected, cf. Hein et al. [1988].

3.2 MODEL DESCRIPTION

The relation between total electron content (TEC) and ionospheric electron density can be written as:

$$\begin{aligned} \text{TEC} &= \int_{rx}^{sat} N_e(l, f, z)\,ds = \\ &\int_{rx}^{sat} [N_e^0(l, f, z) + dN_e(l, f, z)]\,ds \end{aligned} \quad (6)$$

where $N_e(l, f, z)$ is the ionospheric electron density at the geospatial position of (l, f, z). $N_e^0(l, f, z)$ is the a apriori value of $N_e(l, f, z)$ which could be an output from an empirical model that reflects the deterministic portion of our a apriori information. $dN_e(l, f, z)$ is the correction to the a apriori value. l, f, z are longitude, latitude and altitude, respectively, referenced to solar-geomagnetic system. In our study, we can let the $N_e(l, f, z)$ have an approximation of zero, namely $N_e^0(l, f, z) = 0$, for the convenience purpose. Thus we have,

$$\text{TEC} = \int_{rx}^{sat} dN_e(l, f, z)\,ds \quad (7)$$

The correction for electron density function, $dN_e(l, f, z)$ can be modeled by a series of space-location related functions. More specifically we can employ spherical harmonic expansions in horizon and empirical orthogonal functions (EOFs) vertically to model the ionospheric electron correction term. The spherical harmonic expansion is better than 2D grid model when the model is used for a large area ionospheric modeling. The empirical orthogonal functions are used for vertical profile description. The integration of these two sets of functions enables us to depict the ionosphere field in a 3D mode.

$$dN_e(l, f, z) = \sum_{k=1}^{K} \sum_{m=-M}^{M} \sum_{n=|m|}^{M} [a_{nk}^m \cos(ml) + b_{nk}^m \sin(ml)] \bar{P}_n^m(\cos f) Z_k(z) \quad (8)$$

where $\bar{P}_n^m(\cos f)$ is the associated Legendre polynomial of order m and degree n; $Z_k(z)$ is the empirical orthogonal function (EOF); a_{nk}^m and b_{nk}^m are the coefficients we are to estimate. Other parameters are defined as Eq. (6). Combining Eq. (7) and (8), the observation equation for ionospheric 3D modeling is established.

$$\begin{aligned} \text{TEC} &= \int_{rx}^{sat} \sum_{k=1}^{K} \sum_{m=-M}^{M} \sum_{n=|m|}^{M} [a_{nk}^m \cos(ml) + b_{nk}^m \sin(ml)] \bar{P}_n^m(\cos f) Z_k(z)\,ds \\ &= \sum_{k=1}^{K} \sum_{m=-M}^{M} \sum_{n=|m|}^{M} a_{nk}^m \int_{rx}^{sat} \cos(ml) \bar{P}_n^m(\cos f) Z_k(z)\,ds + \\ &\quad \sum_{k=1}^{K} \sum_{m=-M}^{M} \sum_{n=|m|}^{M} b_{nk}^m \int_{rx}^{sat} \sin(ml) \bar{P}_n^m(\cos f) Z_k(z)\,ds \end{aligned} \quad (9)$$

Equation (9) is the fundamental observation equation for 3D ionospheric modeling using tomography inversion technique, through which the GPS derived total electron content (TEC) and the coefficients describing the ionosphere field are linked. The following task associated with the observation equation is the estimation of the model parameters. The number of model parameters is a function of the truncation limit of the expansions.

3.3 PARAMETER ESTIMATION

The parameters a_{nk}^m and b_{nk}^m, which define the ionospheric field expressed in the above Eq. (9), are the unknowns needing to be estimated. Generally the equation for parameter estimation has the following matrix expression [Fremouw et al., 1992, 1994]:

$$d = Gm + n \tag{10}$$

where d is the data vector, namely the TEC measurements; and m is the model vector, the elements of which are the parameters a_{nk}^m and b_{nk}^m to be estimated. Matrix G is geometry matrix describing the dependence of the data on the model parameters, with elements $G_{hk} = \partial d_h / \partial m_k$. The elements of noise vector n quantify the uncertainty of the measurements in the data vector d.

Whatever means one selects to set up the matrix equation, the fundamental task is to inverse it as efficiently and accurately as possible. The standard least squares inversion technique minimizes the square of the difference between the data vector computed by means of Eq. (10) and the data actually observed. That is, it minimizes the "prediction error," which is appropriate when the inversion problem is overdetermined. Often some model elements are overdetermined and some are underdetermined (the "mix-determined" problem). To damp the underdeterminacy in this common situation, the " damped least squares technique" is used. Combining weighting and damping yields the so-called weighted, damped least squares technique, which is adopted in this study [Fremouw et al., 1992]. The means by which the equation (10) is inversed is application of a generalized inversion of G, as defined in Menke [1989]. The weighted, damped least squares technique applies the following generalized inversion operator to the data:

$$G^{-g} = VG^T (GVG^T + E)^{-1} \tag{11}$$

where G^T is the transpose of G and where V and E are the covariance matrices of m and n, respectively. Once G^{-g} is computed, the model coefficient vector estimate can be readily obtained by:

$$\hat{m} = G^{-g} d \tag{12}$$

Since G depends only on the configuration of the experiment, therefore it can be computed whenever the experiment situation is known. This is helpful when the real-time ionosphere tomography is required.

4 EXPERIMENT AND DATA ANALYSIS

Experiment is done with the data from 11 GPS stations excerpted from Southern California Integrated GPS Network (SCIGN). SCIGN is designed to provide geophysical information for the earthquake prediction and crustal deformation monitoring in the Southern California area through the processing of GPS data. The distribution of GPS stations used in this study is shown in Figure 1. The geographical coverage of the 11 sites is from 117.8 to 118.8 degree in west longitude and from 33.8 to 34.5 degree in north latitude.

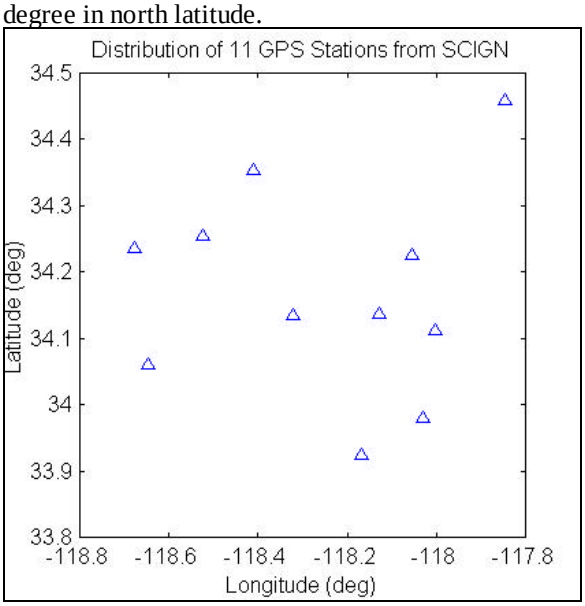

Figure 1. Distribution of 11 GPS sites in SCIGN

Since this study is only the preliminary step of the ionosphere tomography modeling and our purpose of this study is to see whether the 3D ionospheric tomography is feasible in implementation, we use the pseudorange measurements only instead of the carrier phase smoothed pseudorange. Also the receiver interfrequency bias is presumed to be zero for the convenience purpose. However, these two simplifications don't influence our results, as we can see in the following section.

4.1 DATA DESCRIPTION

The GPS data collected from 11 stations for May 15 (day of year 136), 2000 are used there. The data sampling rate is 30 seconds. The cutoff elevation used for the calculation of TEC measurements is 15 degrees, which is a widely used cutoff in GPS data processing. Not all the data for that entire day but only two small datasets are extracted from that day

for this experiment since this experiment's purpose is to test how well the ionospheric tomographic model performs in terms of ionospheric delay recovery capability. More specifically, 30 epochs of data collected at local time 16:00 are selected as the first dataset. The second dataset includes also 30 epochs of GPS measurements, but corresponding to local time 14:00, when it is generally believed to have daily largest ionospheric density. In the 30 epochs of period, equivalent to 900 seconds, the ionosphere is presumed frozen. The variation in the ionosphere within this short period of time is not considered in this modeling.

For each dataset, we don't use all 30 epochs of TEC measurements for the model computation. We separate the TEC measurements into two groups. The first group consists of 100 TEC measurements for the model quality checking purpose. We call it check group. The second group, named model group, is comprised of all the rest TEC data which have about 1400 TEC measurements. The data from check group don't participate the model coefficient determination, namely, m vector in Eq. (10). The model coefficients are calculated using the model group data. However the geometry matrix G corresponding to the check group data can be obtained by using the operator $G_{hk} = \partial d_h / \partial m_k$. Based on Eq. (10), the multiplication of G matrix and m vector is the recovered TEC for the check group data, by employing the ionospheric tomographic model determined by the model group data. For the check group data, we actually have already obtained the TEC measurements from dual-frequency GPS data. The GPS-derived TEC measurements are independent of the model-recovered TEC data since the check group and model group are two separate groups of TEC measurements and since check group data are not used for tomographic modeling. Therefore it is meaningful to compare the GPS-derived TEC measurements against the model-recovered TEC data to evaluate the performance of ionospheric tomographic model generated in this study.

4.2 RESULT OF DATASET ONE

The result from the first dataset is given in the following figures. Figure 2 shows the result of model recovery relative error versus the TEC measurement elevation angle. The model recovery relative error is computed by:

$$R.E = \frac{TEC_{GPS} - TEC_{\text{model}}}{TEC_{GPS}} \times 100\% \qquad (12)$$

where TEC_{GPS} and TEC_{model} are the TEC values derived from GPS data and ionospheric model, respectively. It can be seen the magnitude of relative error is roughly inversely proportional to the value of elevation angle. For TEC measurement with high elevation, its corresponding relative error is small. Figure 2 indicates that the magnitudes of relative error of ionospheric model recovery vary between 0.01% and 47.06%. The mean magnitude of the relative errors is 9.41%. Among these results, 80% of them have a magnitude of relative error less than 15%. The three peak relative errors correspond to the TEC measurements with lowest elevations. This implies the ionospheric tomographic model has a recovery capability of over 90%. This is especially beneficial for the single frequency GPS receiver users who can only correct about 50% ionospheric error using broadcast Klobuchar model coefficients.

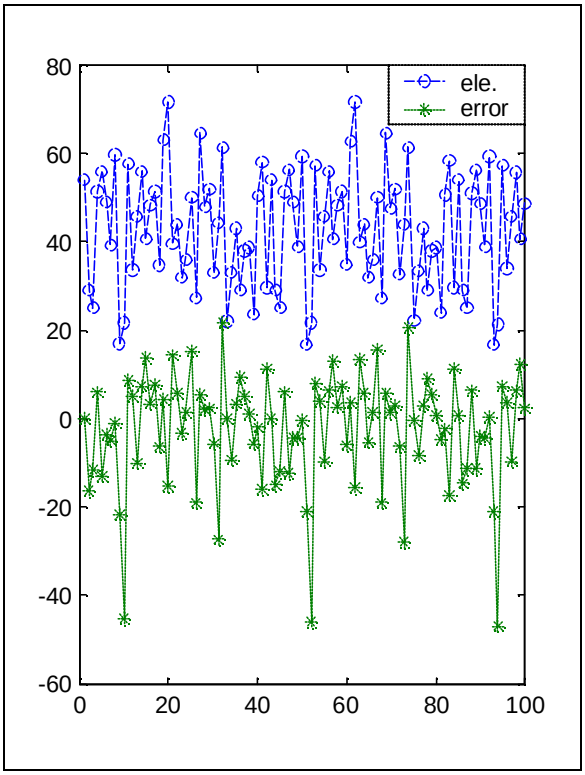

Figure 2. Relative TEC error versus elevation angle. TEC measurements collected at Local Time 16:00. The upper panel indicates the elevation angles in degree of the 100 TEC checking measurements. The lower panel indicates their relative errors obtained by comparing with GPS-derived values.

4.3 RESULT OF DATASET TWO

The second set of TEC data were collected at local time 14:00. It is thought at this time, the ionosphere electron density has the highest value. To test the validity and performance of this tomography model under the extreme condition, computation experiment similar to the above is conducted. The relative error of each checking measurement is computed by Eq. (12) and is plotted versus their elevations in Figure 3. The minimum magnitude of relative recovery error is 0.003% and the maximum is 42.09%. The average size of relative error is 10.20%. It is noticeable there are a few checking data whose relative recovery errors have much larger values than other data. Comparing the relative error against the elevation angle, it is easily identified all these peak values almost correspond to relatively low elevation angles.

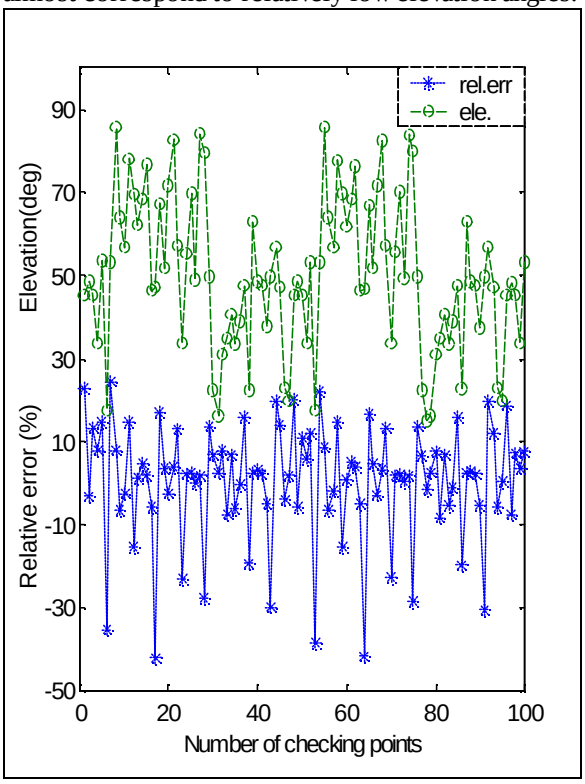

Figure 3. Relative TEC error versus elevation angle. TEC measurements collected at Local Time 14:00. The upper panel indicates the elevation angles in degree of the 100 TEC checking measurements. The lower panel indicates their relative errors obtained by comparing with GPS-derived values.

It can be seen this model performs under extreme ionospheric condition almost the same well as it does in the regular ionospheric condition. At the same time it should be noticed that the elevation angles for the checking data in dataset two are generally larger than those in dataset one. The minimum elevation angle in dataset two is 17.8 degrees and the highest elevation is 86.2 degrees. The mean elevation is 51.4 degrees. While in dataset one, the lowest and highest elevations are 16.7 and 71.8 degrees, respectively. The mean elevation is 42.9 degrees. The generally high elevations in dataset two may contribute to the good model recovery capability although the model is implemented under the extreme ionospheric condition.

Using the model coefficients, the ionosphere electron density for a given spatial point can be calculated. The ionosphere electron densities for various layers above the surface of the Earth are computed with the model coefficients obtained from dataset two. The first layer starts from the height of 100km and the other 4 layers are computed with a height increase of 100km for each layer.

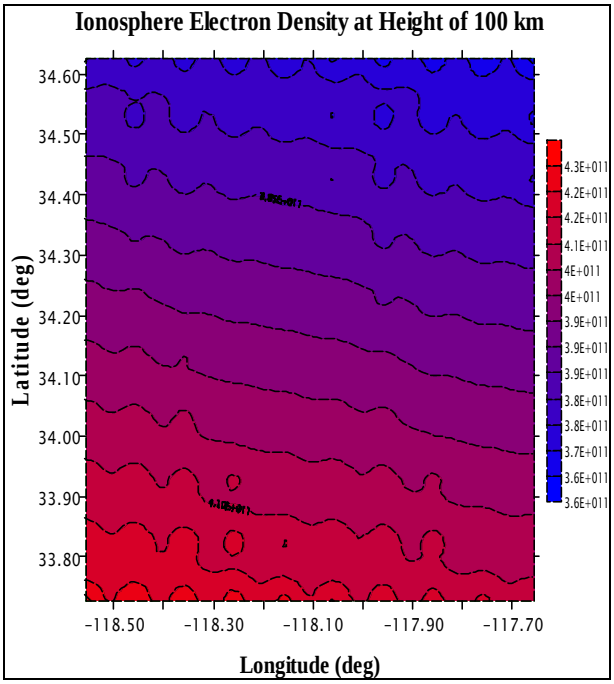

Figure 4. Ionosphere electron density distribution at height of 100km

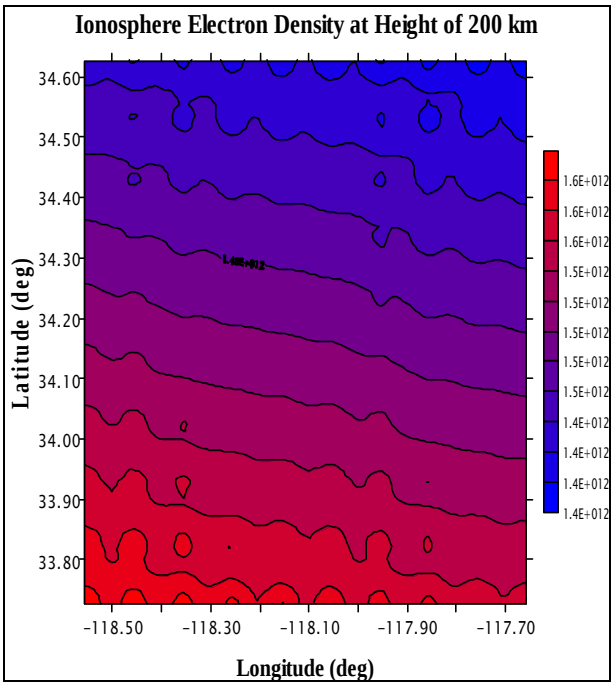

Figure 5. Ionosphere electron density distribution at height of 200km

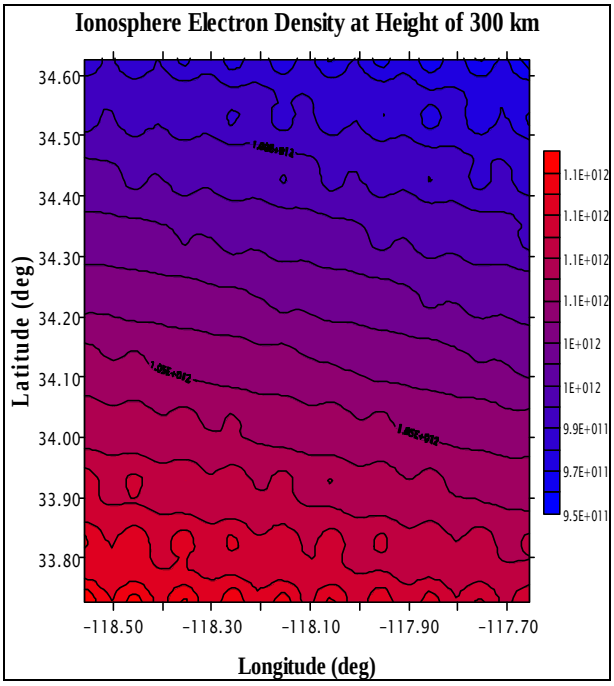

Figure 6. Ionosphere electron density distribution at height of 300km

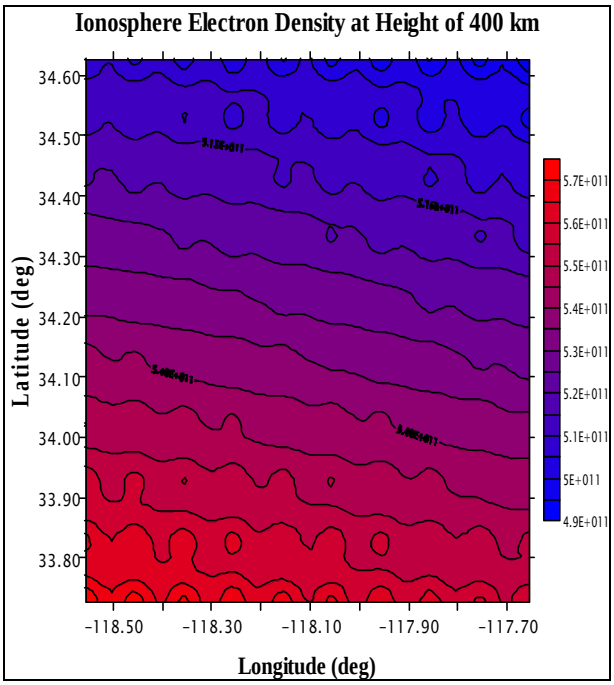

Figure 7. Ionosphere electron density distribution at height of 400km

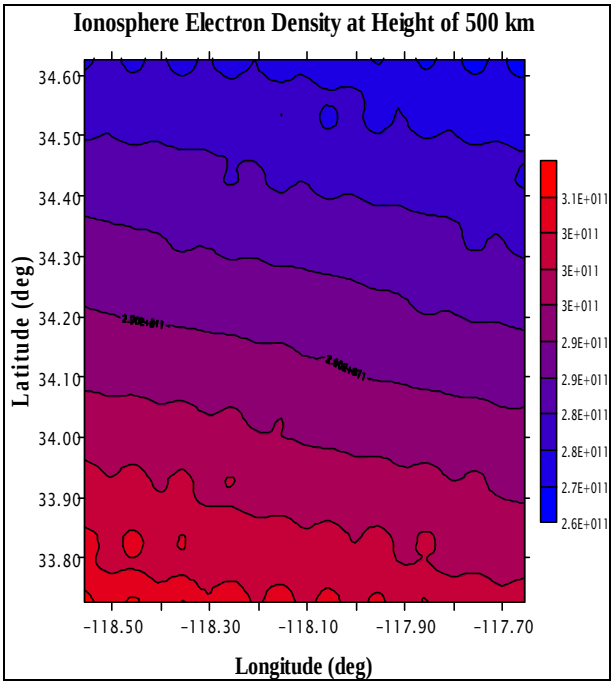

Figure 8. Ionosphere electron density distribution at height of 500km

Comparing the Figures 4 to 8, it can be seen the maximum electron density occurs at a height between 200km and 300km above the surface of the Earth. At different heights, all the Figures indicate a common feature that at lower latitude, the electron density appears to be larger.

5 CONCLUSIONS

The results from two datasets indicate that the tomographic model can recover about 90% ionospheric delay even if the ionospheric model is established based on using pseudorange GPS measurements. Higher recovery capability is expected when carrier phase measurement is used for model construction. The results show that the tomographic model performance has no significant difference under extreme and normal ionospheric conditions. This is validated by the consistency in the relative recovery errors obtained under these two scenarios. The results indicate the capacity of the model's recovering ionosphere has a correlation with the elevation angle GPS signals. When GPS signal has a high elevation, the recovering error generated by the model is usually small.

Figures 4 to 8 validate that the 3D ionospheric tomography model is a good tool to reconstruct the ionosphere electron density at various heights above the Earth surface. These ionosphere electron density data may be assimilated with other ionosphere related data to produce more convincing results.

ACKNOWLEDGEMENTS

This research was supported by Natural Sciences and Engineering Research Council of Canada (NSERC).

The Southern California Integrated GPS Network and its sponsors, the W.M. Keck Foundation, NASA, NSF, USGS, SCEC, are thanked for providing data used in this study.

REFERENCES

Andreeva, E.S., V.E. Kunitsyn, and E.D. Tereshchenko (1992), Phase difference radiotomography of the ionosphere. *Ann. Geophysicae*, 10, 849-855.

Austen, J.R., S.J. Franke, and C.H. Liu (1988), Ionospheric imaging using computerized tomography. *Radio Science*, 23, 299-307.

Austen, J.R., S.J. Franke, C.H. Liu, and K.C. Yeh (1986). Application of computerized tomography techniques to ionospheric research, URSI and COSPAR International Beacon Satellite Symp. On Radio Beacon Contribution to the Study of Ionization and Dynamics of the Ionosphere and to corrections to geodesy and technical workshop, June 9-14, 1986 in Oulu, Finland, *Proceedings Part 1*, 25-35, edited by A. Tauriainen, University of Oulu, ISBN 951-42-2256-3.

Brunner, Fritz K., and Min Gu (1991), An improved model for the dual frequency ionospheric correction of GPS observations. *Manuscripta geodaetica*, Vol. 16, 205-214.

El-Arini, M.B., P.A. O'Donnell, P. Kellam, J.A. Klobuchar, T.C. Wisser, and P.H. Doherty (1993), The FAA Wide Area Differential GPS (WADGPS) Static Ionospheric Experiment, Proceedings of The Institute of Navigation National Technical Meeting, San Francisco, CA, January, 1993.

El-Arini, M.B., C.J. Hegarty, J.P. Fernow, and J.A. Klobuchar (1994a), Development of an Error Budget for a GPS Wide-Area Augmentation System (WAAS), Proceedings of The Institute of Navigation National Technical Meeting, San Diego, CA, January, 1994.

El-Arini, M.B., R.S. Conker, T.W. Albertson, J.K. Reagan, J.A. Klobuchar, and P.H. Doherty (1994b), Comparison of Real-Time Ionospheric Algorithms for a GPS Wide-Area Augmentation System (WAAS), Navigation, Journal of The Institute of Navigation, Vol. 41, No. 4, 393-413.

Fremouw, E.J., J.A. Secan, and B.M. Howe (1992), Application of stochastic inverse theory to ionospheric tomography. *Radio Science*, 27, 721-732.

Fremouw, E.J., J.A. Secan, R.M. Bussey, and B.M. Howe (1994), A status report on applying discrete inverse theory to ionospheric tomography. International Journal of Imaging Systems and Technology, Vol.5, 97-105.

Gao, Y., P. Heroux, and J. Kouba (1994), Estimation of GPS receiver and satellite L1/L2 signal delay biases using data from CACS. Proceedings of the International Symposium on Kinematic Systems in Geodesy, Geomatics and Navigation, 109-117, August 30-September 2, Banff, Canada.

Hansen, Andrew J., Todd Walter, and Per Enge (1997), Ionospheric Correction Using Tomography. *Proceedings of the Institute of Navigation GPS 97*, The Satellite Division of The Institute of Navigation 10th International Technical Meeting, September16-

19, 1997, Kansas City Convention Center, Kansas City, Missouri, USA.

Hargreaves, J.(1992), The Solar-Terrestrial Environment. Cambridge: Cambridge University Press.

Hatch, R. (1982), The synergism of GPS code and carrier measurements. Proceedings of the Third International Symposium on Satellite Doppler Positioning, New Mexico State University, Feburary 8-12, Vol. 2: 1213-1231.

Hein, G.W., H. Landau, and G. Baustert (1988), Terrestrial and aircraft differential kinematic GPS positioning. Groten. E, StraußR (eds): GPS - techniques applied to geodesy and surveying. Springer, Berlin Heidelberg New York London Paris Tokyo, 307-348 [Bhattacharji S., G.M. Friedman, H.J. Neugebauer, and A. Seilacher (eds): Lecture Notes in Earth Sciences, Vol 19].

Howe, Bruce M. (1997), 4-D Simulations of Ionospheric Tomography. *Proceedings of ION*, National Technical Meeting, 269-278.

Howe, Bruce M., K. Runciman, and J. A. Secan (1998), Tomography of ionosphere: Four-dimensional simulations. *Radio Science*, Volume 33, No. 1, 109-128.

King, R.W., E.G. Master, C. Rizos, A. Stolz, and J. Collins (1985), Surveying with GPS, 128pp., Dümmler, Bonn.

Klobuchar J. (1986), Design and characteristics of the GPS ionospheric time-delay algorithm for single-frequency users. In: *Procedings of the IEEE Position Location and Navigation Symposium*, Las Vegas, November 4-7.

Liao, Xiangqian (2000), Carrier Phase Based Ionosphere Recovery Over A Regional Area GPS Network, UCGE Reports, Number 20143, University of Calgary, Calgary, Alberta, Canada, pp120.

Kersley, L., J.A.T. Heaton, S.E. Pryse, and T.D. Raymund (1993), Experimental ionospheric tomography with ionosonde input and EISCAT verification, *Ann. Geophysicae*, 11, 1064-1074.

Klobuchar, John A., and Joseph M. Kunches (2000), Eye on the Ionosphere: Correcting for Ionospheric Range Delay on GPS---Temporal Decorrelation. *GPS Solutions*, Vol. 3, No.2. 78-82.

Kutzbach, J.E. (1967), Empirical eigenvectors of sea-level pressure, surface temperature and precipitation complexes over North America, *J. Appl. Meter*., 6, 791.

Komjathy, A. (1997), Global Ionospheric Total Electron Content Mapping Using the Global Positioning System, Ph.D. dissertation, Department of Geodesy and Geomatics Engineering Technical Report NO. 188, University of New Brunswick, Fredericton, New Brunswick, Canada, 248pp.

Lachapelle, G., J. Hagglund, W. Falkenberg, P. Bellemare, M. Casey, and M. Eaton (1986), GPS land kinematic positioning experiments. Proceedings of the Fourth International Geodetic Symposium on Satellite Positioning, Austin, Texas, April 28-May 2, Vol 2: 1327-1344.

Lorentz, E.N. (1956), Empirical orthogonal functions and statistical weather prediction, *Sci. Rep. No.1*, Contract AF19(604)1566, AFCRC-TN-57-256, Dept. Meteor., MIT.

Menke, W. (1989), Geophysical data analysis: discrete inverse theory, Academic, San Diego, California.

Odijk, Dennis, Hans van der Marel, and Inseong Song (2000), Precise GPS Positioning by Applying Ionospheric Corrections from an Active Control Network. *GPS Solutions*, Vol.3, No.3, 49-57.

Parkinson, B.W., and J. Spilker (1996) eds. Global Positioning System: Theory and Application. Washington D.C.: AIAA.

Raymund, T.D. (1995), Comparisons of several ionospheric tomography algorithms. *Ann. Geophys.*, 13, 1254-1262.

Raymund, T.D., J.R. Austen, S.J. Franke, C.H. Liu, J.A. Klobuchar, and J. Stalker (1990), Application of computerized tomography to the investigation of ionospheric structures. *Radio Science*, 25, 771-789.

Raymund, T.D., Y. Bresler, D.N. Anderson, and R.E. Daniell (1994), Model-assisted ionospheric tomography: A new algorithm. *Radio Science*, 29, 1493-1512.

Secan, James A., and Thomas F. Tascione (1984), The 4D ionospheric objective analysis model. *Proceedings of the conference on the Effects of the ionosphere on C^3I system*, J. Goodman, ed., 336-345, NTIS, Spring-field, VA.